Three-nucleon force effects in 3N hadronic and photonic reactions

H. Witała*, R. Skibiński*, J. Golak*, W. Glöckle†, H. Kamada**, A. Nogga‡ and W.N. Polyzou§

*M. Smoluchowski Institute of Physics, Jagiellonian University, PL-30059 Kraków, Poland
†Institut für Theoretische Physik II, Ruhr-Universität Bochum, D-44780 Bochum, Germany
**Department of Physics, Faculty of Engineering, Kyushu Institute of Technology, 1-1 Sensuicho Tobata, Kitakyushu 804-8550, Japan
‡Forschungszentrum Jülich, Institut für Kernphysik (Theorie), D-52425 Jülich, Germany
§Department of Physics and Astronomy, The University of Iowa, Iowa City, Iowa 52242, USA

Abstract. Results on three-nucleon (3N) elastic scattering and breakup below the pion production threshold are discussed with emphasis on the need of a three-nucleon force (3NF). The large discrepancies found between a theory based on numerical solutions of 3N Faddeev equations with modern NN potentials only and data point to the action of 3NF's. Successes and failures of the present 3NF models mostly of a 2π-exchange nature to describe high precision 3N data are discussed. Effects due to relativity both in elastic nucleon-deuteron (Nd) scattering and breakup reaction are presented and consequences for 3NF study pointed out. As an application of 3N bound and scattering states results for photodisintegration of 3N bound states are shown.

Keywords: nucleon-nucleon potential, three-nucleon force, elastic scattering, breakup, photodisintegration, pd capture
PACS: 21.45.+v; 21.10.-k; 25.10.+s; 25.20.-x

INTRODUCTION

Traditionally in nuclear physics the Hamiltonian has been taken in a nonrelativistic form in which pairwise interactions between nucleons are supplemented by 3NF's for systems with more than two nucleons. The construction of NN potentials guided by meson theory led to generation of realistic NN interactions which describe the NN data set with high precision (χ^2/datum ≈ 1) [1, 2, 3]. The 3N system is the first nontrivial case where those realistic potentials can be tested. In that system also the first time 3NF's come into play making it a valuable source of information on 3NF properties and their significance in the nuclear Hamiltonian.

The first time 3NF's were established when three- and four-nucleon bound states have been solved exactly using standard integration and differentiation mehtods [4, 5]. Later using stochastic techniques low energy states for nuclei up to A=8 have been calculated [6]. It turned out that in all cases studied realistic NN forces alone provided clear underbinding, which for ^{3}H and ^{3}He amounts to $\approx 0.5-0.9$ MeV and for ^{4}He to $\approx 2-4$ MeV.

It was natural to look for an explanation of this underbinding introducing 3NF's in the nucleonic Hamiltonian. An important example for a process which leads to a 3NF is the $\pi-\pi$ exchange between three nucleons with an intermediate Δ excitation of one nucleon, considered by Fujita-Miyazawa [7]. Later this process was incorporated into Urbana IX 3NF, where it is supplemented by a phenomenological short-range spin- and isospin-independent part [8]. The Tucson-Melbourne (TM) model [9] was constructed using more general πN amplitude. It also contains a strong form factor parametrization with a cut-off parameter Λ which can be adjusted to the ^{3}H or ^{3}He binding energy when this 3NF is combined with particular NN interaction. For the combination of the AV18 NN potential and the Urbana IX 3NF calculations are available for nuclei up to $A = 8$ which show that one can reach a reasonable description of the low lying bound states in those nuclei [6]. However, the results show for instance an insufficient spin-orbit splitting and an insufficient charge dependence, which indicate defects of this 3NF. Taking additional 3NF ring-diagrams into account the situation could be improved [10].

A rich set of spin observables for elastic Nd scattering and the breakup reaction offers itself as a source of valuable information on the spin and momenta structure of 3NF's. In the next section we briefly review the 3N scattering formalism and give some examples where data are compared to various NN potential predictions alone or combined with different 3NF's. These examples are chosen to show importance of the 3NF in the 3N system. The importance of 3NF's seems to increase with increasing energy of 3N system. Therefore we discuss importance of relativistic effects in these reactions and their significance to study 3NF effects. As an application of rigorous 3N bound and scattering states we discuss next the photodisintegration of 3N bound states and the proton-deuteron (pd) capture process. In the last section we give summary.

REACTIONS IN 3N CONTINUUM

All observables for elastic Nd scattering and the breakup reaction can be obtained from an amplitude $T|\phi\rangle$ which fulfills the 3N Faddeev equation [11]

$$\begin{aligned} T|\phi\rangle &= tP|\phi\rangle + (1+tG_0)V_4^{(1)}(1+P)|\phi\rangle + tPG_0T|\phi\rangle \\ &+ (1+tG_0)V_4^{(1)}(1+P)T|\phi\rangle \ . \end{aligned} \tag{1}$$

The initial channel state $|\phi\rangle$ is composed of a deuteron and a momentum eigenstate of the projectile nucleon. On top of 2N forces with their off-the-energy shell t-matrix t, also 3NF is included and $V_4^{(1)}$ is a part of it which is symmetrical under exchange of nucleons 2 and 3. The permutation operator P takes into account the identity of the nucleons and G_0 is the free 3N propagator.

Using the realistic NN forces: AV18 [1], CD Bonn [2], Nijm I, II, and 93 [3] one gets in general predictions for 3N scattering observables which agree well with data at energies below ≈ 30 MeV. A fairly complete overview of those theoretical predictions in comparison to data is presented in [12, 13]. At higher energies discrepancies develop. They are exemplified for the total neutron-deuteron (nd) cross section in Fig.1 and for the elastic scattering cross section in Fig.2. The large discrepancy between total cross sections obtained with NN forces only seen for energies above ≈ 60 MeV is removed for energies below ≈ 140 MeV when 3NF's which reproduce the experimental triton binding energy are included. Also the large discrepancy in the minimum of the elastic scattering cross section using NN forces only is removed when these 3NF's are

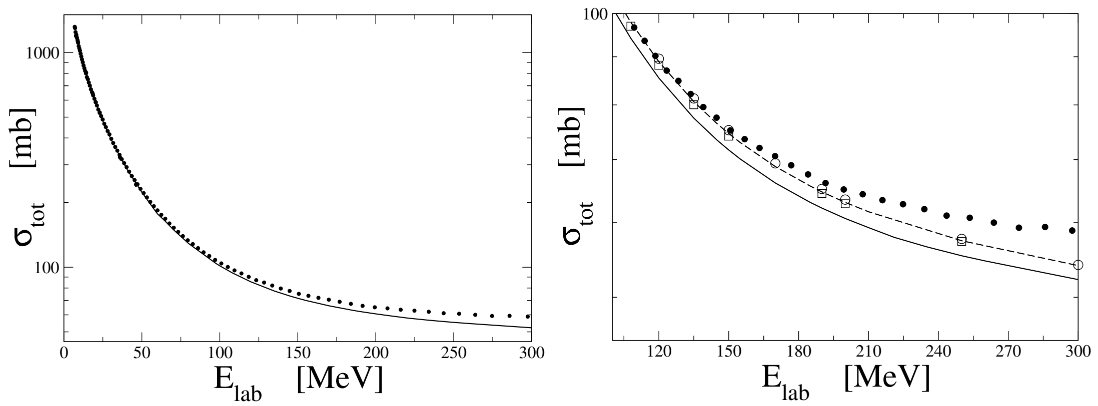

FIGURE 1. The total cross section for nd interaction as a function of incoming neutron lab energy E_{lab}. Experimental data are from [14]. The solid and dashed lines are the CD Bonn and CD Bonn+TM 3NF predictions. The open squares and circles are the results of AV18+Urbana IX 3NF and CD Bonn+TM99 citetm99 3NF predictions.

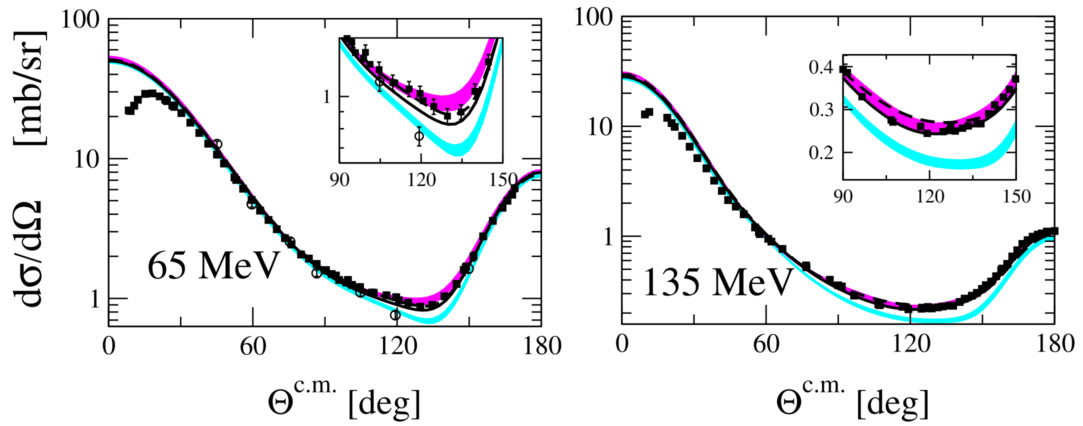

FIGURE 2. Angular distribution of elastic Nd scattering. The light shaded band contains theoretical predictions of the AV18, CD Bonn, Nijm I, II, and Nijm 93 potentials. The dark band contains predictions when these potentials are combined with TM 3NF. The solid and dashed lines are the AV18+Urbana IX and CD Bonn+TM99 predictions. Open circles are 65 MeV nd data from [16]. Full squares are 65 MeV pd data from [17] and 135 MeV pd data are from [18].

included [19, 13]. A similar behavior shows the high energy deuteron vector analyzing power $A_y(d)$ [13, 20, 18] (see Fig.3). But there are many spin observables for which large 3NF effects are predicted and where the TM and the Urbana IX do not reproduce the data [13]. This is the case e.g. for the nucleon analyzing power A_y [13, 22] (see Fig.3). Similar happens for the tensor analyzing powers [13] (see Fig.4). In both cases the data cannot be reproduced by pure 2N force predictions either.

The Nd breakup reaction in specific kinematically complete configurations is also very promising to provide information on the nuclear Hamiltonian and cross sections and some spin observables exhibit very large 3NF effects at higher energies, which moreover are different for the TM and Urbana IX models [23]. Also large discrepancies between

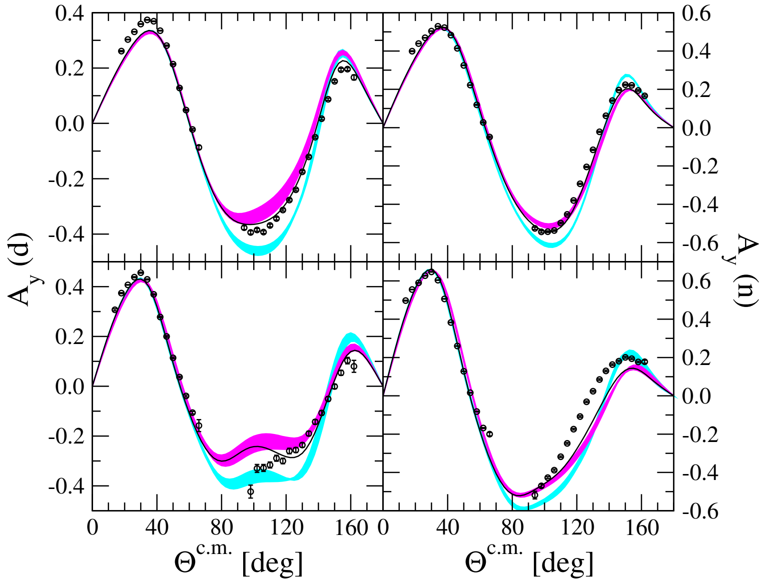

FIGURE 3. The deuteron $A_y(d)$ and neutron $A_y(n)$ vector analyzing powers in elastic nd scattering at incoming neutron lab energy $E = 135$ MeV (first row) and $E = 190$ MeV (second row). Circles are the pd data from [21]. The light bands contain the NN force predictions: AV18, CD Bonn, Nijm I and II. The dark bands contain the combinations of the NN+TM99 3NF predictions. The solid curve is the AV18+Urbana IX 3NF prediction.

high energy breakup cross section data and theory based on NN forces only are found which cannot be removed by adding tM or Urbana IX 3NF's [23] (see Fig.5. Therefore observables of elastic Nd scattering and the breakup process can be identified, which are sensitive to the 3NF structure. With precise data on such spin observables it should be possible to reveal the proper spin structure of the 3NF. It should be pointed out that presently the breakup data base is more restricted than the data base for elastic scattering.

RELATIVISTIC EFFECTS IN 3N CONTINUUM

There are large discrepacies at higher energies between data and theory, both in elastic Nd scattering and breakup reaction, which cannot be removed by adding standard 3NF's (see Fig.1, Fig.5, and Fig.6). They require to study magnitude of relativistic effects. We used an instant form relativistic approach which encompasses relativistic kinematics, boost corrections, and Wigner spin rotations [27, 28]. The boost effects turned out to be the most significant for the elastic scattering cross section at higher energies as shown in Fig.6. They diminish the transition matrix elements at higher energies and lead, in spite of the increased relativistic phase-space factor as compared to the nonrelativistic one, to rather small effects in the cross section, mostly restricted to the backward angles [27].

At energies below ≈ 20 MeV boost and Wigner spin rotation lower the maximum of the nucleon analyzing power A_y increasing the discrepancy between theory and data [28] (see Fig.7). This calls for even larger 3NF effects to explain low energy A_y puzzle.

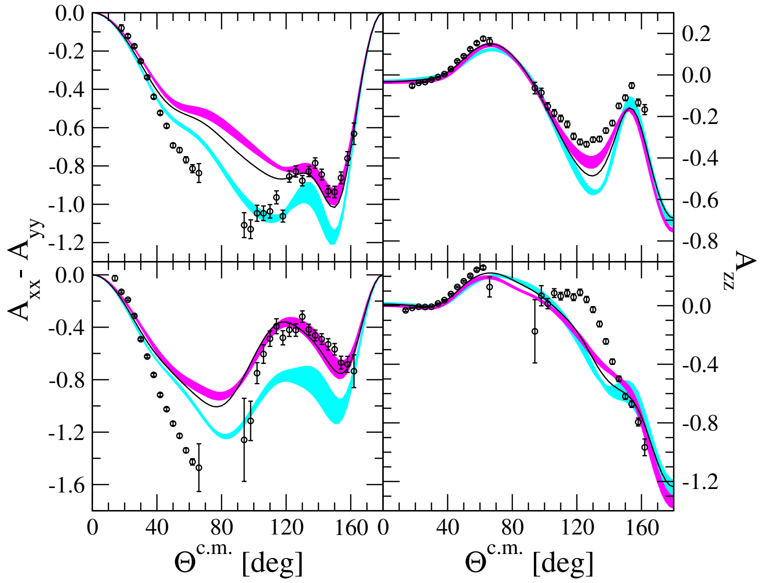

FIGURE 4. The same as in Fig.3 but for tensor analyzing powers $A_{xx} - A_{yy}$ and A_{zz}.

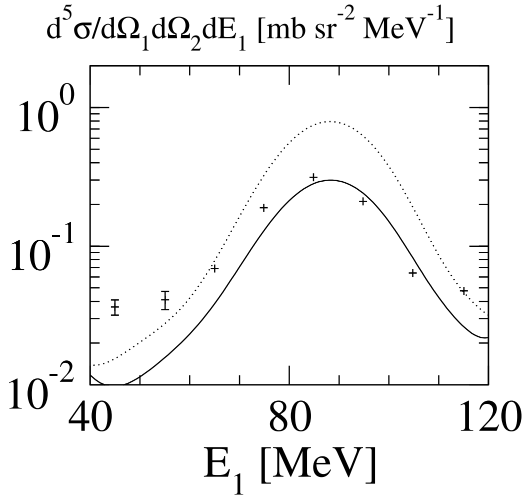

FIGURE 5. The five-fold cross section $\frac{d^5\sigma}{d\Omega_1 d\Omega_2 dE_1}$ for the $d(n,np)n$ breakup reaction at incoming neutron lab energy $E = 200$ MeV. The angles of detected nucleons are: $\theta_1 = 52^o$, $\theta_2 = 45^o$, $\phi_{12} = 180^o$. The $d(p,pn)p$ data are from [24]. The nonrelativistic and relativistic cross sections are shown by dotted and solid lines, respectively.

Higher energy elastic scattering spin observables are only slightly modified by relativity. The selectivity of the breakup singles out this reaction as a tool to look for localized effects which when averaged are difficult to see in elastic scattering. At higher energies this selectivity of breakup allows to find the configurations with large relativistic and/or 3NF effects for the breakup cross section. The configurations with large increasing and decreasing relativistic effects are localized in a specific regions of the breakup phase-

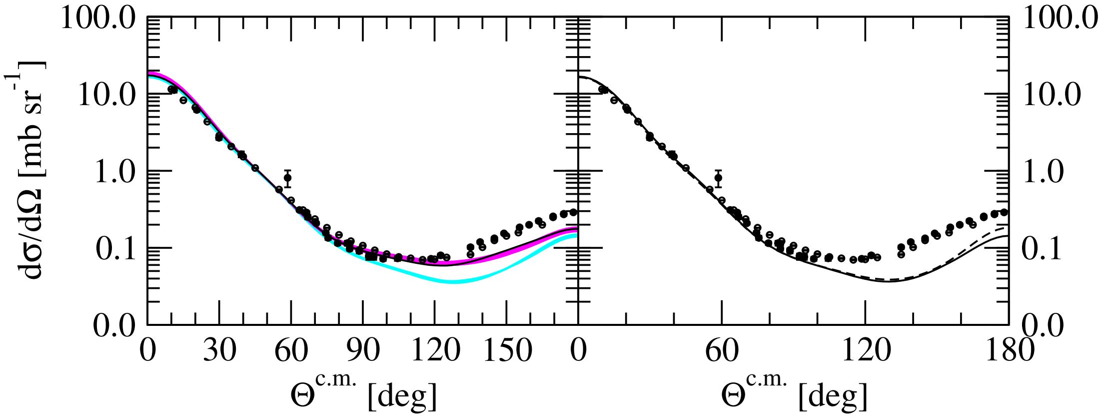

FIGURE 6. The Nd elastic scattering angular distribution at incoming nucleon lab energy $E = 250$ MeV. On the left side the light shaded band contains theoretical predictions of the AV18, CD Bonn, Nijm I and II potentials. The dark band contains predictions when these potentials are combined with TM99 3NF. The solid line is prediction obtained with AV18+Urbana IX 3NF. On the right side the solid line is prediction of the CD Bonn potential and the dashed line is the relativistic result with boost effects included. Open circles are pd data from [25] and solid circles are nd data from [26].

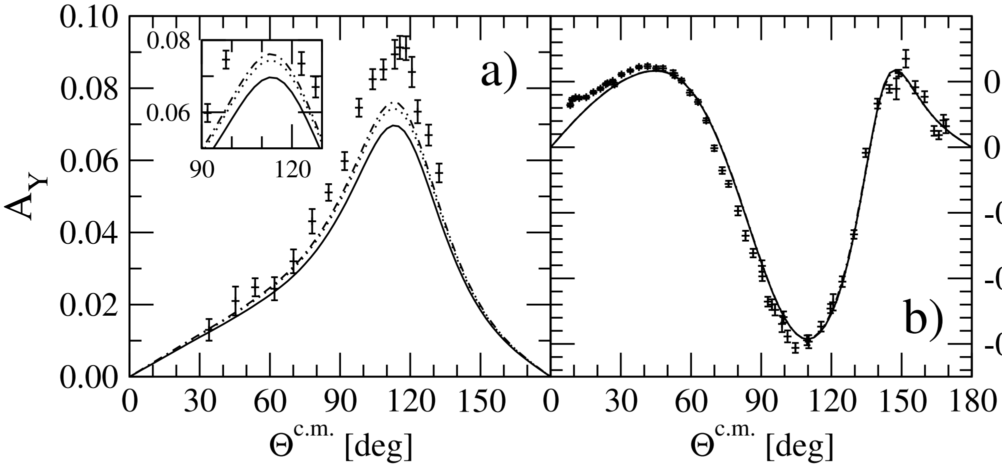

FIGURE 7. The nucleon analyzing power A_y in elastic Nd scattering at $E_{lab}^{N} = 5$ MeV (a) and 65 MeV (b). The dashed-dotted line is nonrelativistic result obtained with CD Bonn potential. The corresponding relativistic predictions are given by dotted and solid lines for the cases without and with Wigner rotations, respectively. The nd data in a) are from [33] and pd data in b) from [17].

space [29, 30] and two cases are exemplified in Fig.8. Some existing data seems to support these relativistic effects [30] (see Fig.5).

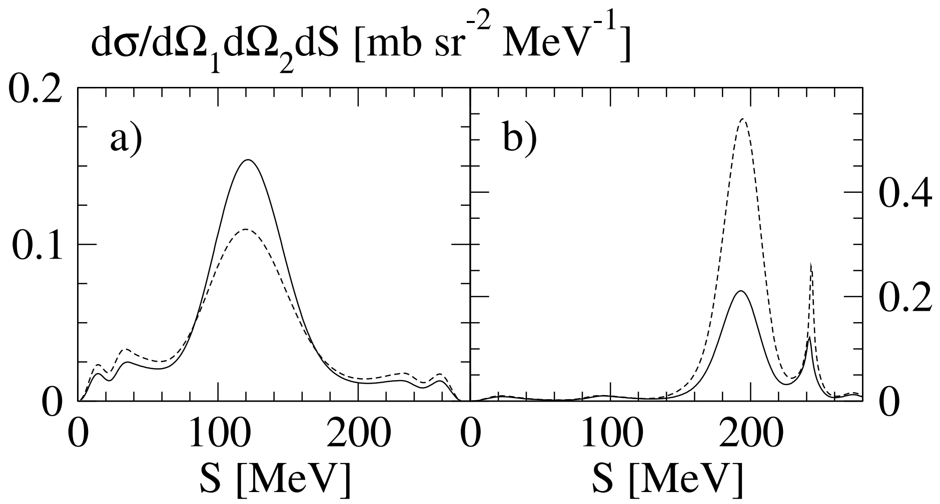

FIGURE 8. The cross section for exclusive d(n,nn)p breakup at $E^n_{lab} = 200$ MeV at fixed angle $\theta_2 = 37.5^o$, $\phi_{12} = 180.0^o$, and varying θ_1: a) $\theta_1 = 32.5^o$, b) $\theta_1 = 62.5^o$. The nonrelativistic and relativistic cross sections are shown by dashed and solid lines, respectively. The calculations are based on the CD Bonn potential.

THE PHOTODISINTEGRATION OF 3N BOUND STATES AND THE PD CAPTURE REACTION

All observables for these electromagnetic processes can be calculated from the nuclear matrix element

$$N_\tau = \langle \Psi_f^{(-)} | j_\tau(\vec{Q}) | \Psi_b M_b \rangle \ . \tag{2}$$

It contains the ^{3}He (^{3}H) bound state $|\Psi_b M_b\rangle$ with spin projection M_b, the spherical components $j_\tau(\vec{Q})$ ($\tau = \pm 1$) of the nuclear current operator defined in relation to the photon momentum $\vec{Q} \parallel \hat{z}$, and the final interacting state $\langle \Psi_f^{(-)}|$. Using the Faddeev decomposition of $\langle \Psi_f^{(-)}|$, N_τ can be calculated using numerical methods in the 3N continuum [31].

We use different electromagnetic current operators. We apply single nucleon current augmented by explicit π- and ρ-like two-body meson exchange currents or employ the Siegert theorem, which induces many-body contributions to the current operator. For fairly complete overview of theoretical predictions in comparison to data we refer to [31, 32].

Cross section for the two-body photodisintegration of ^{3}He reveals clear signature of 3NF. Including 3NF increases this cross section with increasing energy of the incoming photons (see Fig.9). This increase is supported by some existing data as shown in Fig.10

At lower energies the angular distribution for photodisintegration and pd capture are rather well described [31]. However, the effects of final (initial) state interactions are very large. For proton analyzing powers there are some discrepancies at low and higher energies [31].

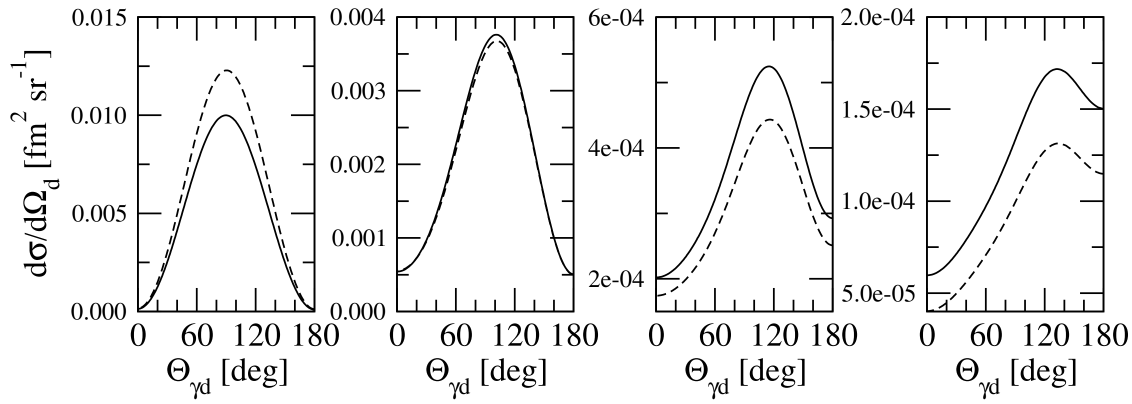

FIGURE 9. The angular distributions of deuterons from 2-body photodisintegration of ^{3}He at two photon energies. $\Theta_{\gamma d}$ is the lab. angle of outgoing deuterons. The dashed (solid) lines show the result of AV18 (AV18+Urbana IX) Siegert calculations.

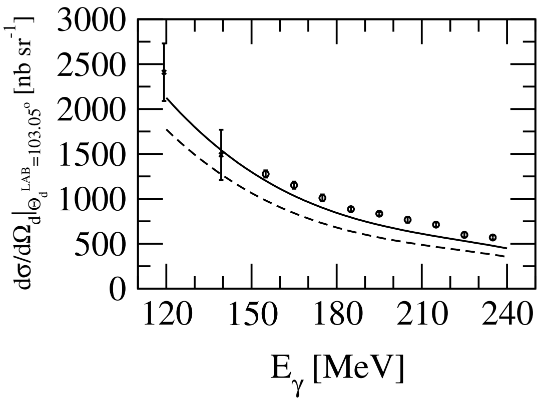

FIGURE 10. Deuteron angular distribution for the process ^{3}He(γ,d)p at $\theta_d^{lab} = 103.5^o$ as a function of the photon energy E_γ. Lines show results of calculations with the AV18 alone (dashed) and with the AV18 + Urbana IX (solid). Explicit π- and ρ-like MEC's are included in the current operator. Data are from [34] (x-es) and [35] (circles).

At higher energies the descrepancies between the cross section data and theory resembles that for elastic Nd scattering. Including 3NF improves the description of data. However, the theoretical predictions depends on the current operator used (see Fig.11). For the proton analyzing power the influence of the 3NF is smaller but results also depend strongly on the current used (Fig.12).

SUMMARY

Solving 3N scattering exactly in a numerical sense up to energies below the pion production threshold allows to test 3N Hamiltonian based on modern NN potentials and 3NF's. At the higher energies for some observables large 3NF effects are predicted when using present day models such as TM and Urbana IX. Some Nd elastic scattering

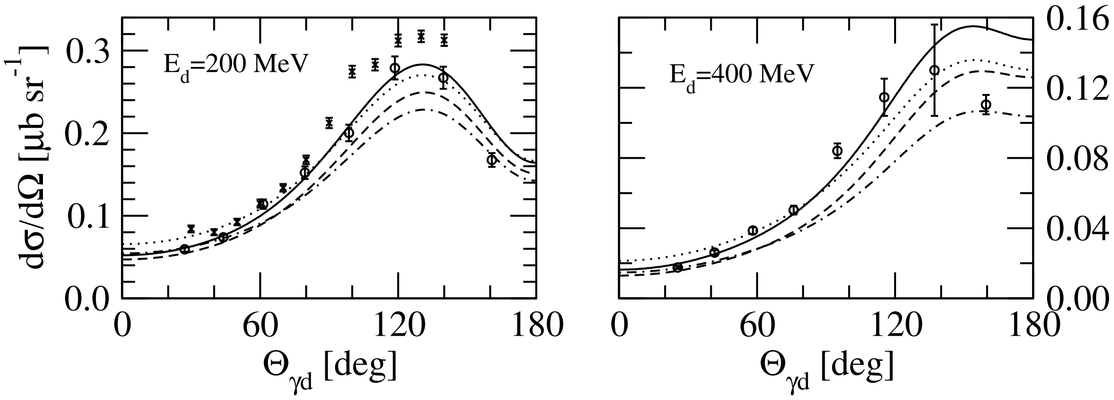

FIGURE 11. The c.m. pd capture cross sections at two deuteron lab energies calculated with four different dynamical inputs: MEC + AV18 (dashed line), Siegert + AV18 (dot-dashed line), MEC + AV18 + Urbana IX (solid line), Siegert + AV18 + Urbana IX (dotted line). Data at 200 MeV are from [36] (circles) and [37] (x-es). At 400 MeV they are from [36].

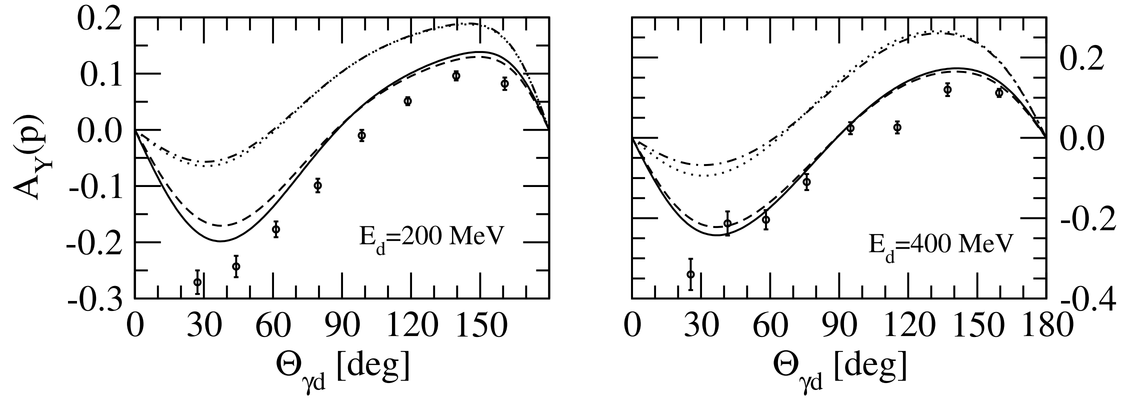

FIGURE 12. The proton anlyzing power A_y in pd capture at a) 200 MeV and b) 400 MeV deuteron lab energies. Lines and data as in Fig.11.

cross sections and polarization data support these predictions. Others, however, indicate defects of present day 3NF's. It can be expected that a precise and rich data basis, comprising elastic scattering and breakup data, will enable to establish the proper spin structure of 3N forces.

Relativistic effects are found to be small for elastic scattering cross section. In case of breakup reaction their importance depends on the phase-space region studied. The existing high energy discrepancies which remain even when Urbana IX or TM 3NF's are included indicate on importance of short-range contributions to a 3NF.

A well founded 3N Hamiltonian is a prerequisite for a theoretical analysis of electroweak processes in 3N systems. Exact 3N bound and scattering states are mandatory in such an analysis to account for the final state interactions. Results depend on the electromagnetic current operator used.

Chiral perturbation theory providing consistent NN and 3N forces [38] together with consistent electromagnetic current operator will play an important role in these studies.

ACKNOWLEDGMENTS

The numerical calculations were performed on the IBM Regatta p690+ of the NIC in Jülich, Germany.

REFERENCES

1. R. B. Wiringa, V. G. J. Stoks, R. Schiavilla, Phys. Rev. C**51**, 38 (1995).
2. R. Machleidt, Phys. Rev. C**63**, 024001 (2001).
3. V. G. J. Stoks et al., Phys. Rev. C**49**, 2950 (1994).
4. A. Nogga, H. Kamada, W. Glöckle, Phys. Rev. Lett. **85**, 944 (2000).
5. M. Viviani, Nucl. Phys. **A631**, 111c (1998).
6. R. B. Wiringa et al., Phys. Rev. C**62**, 014001 (2000).
7. J. Fujita, H. Miyazawa, Prog. Theor. Phys. **17**, 360 (1957).
8. B. S. Pudliner et al., Phys. Rev. C**56**, 1720 (1997).
9. S. A. Coon et al., Nucl. Phys. **A317**, 242 (1979); S. A. Coon, W. Glöckle, Phys. Rev. C**23**, 1970 (1981).
10. S. C. Pieper et al., Phys. Rev. C**70**, 054325 (2004).
11. D. Hüber et al., Acta Phys. Polonica **B28**, 167 (1997).
12. W. Glöckle et al., Phys. Rep.**274**, 107 (1996).
13. H. Witała et al., Phys. Rev. C**63**, 024007 (2001).
14. W. Abfalterer et al., Phys. Rev. Lett. **81**, 57 (1998).
15. S. A. Coon and H. K. Han, Few-Body Systems **30**, 131 (2001).
16. H. Rühl et al., Nucl. Phys. **A524**, 377 (1991).
17. H. Shimizu et al., Nucl. Phys. **A382**, 242 (1982).
18. H. Sakai et al., Phys. Rev. Lett. **84**, 5288 (2000).
19. H. Witała et al., Phys. Rev. Lett. **81**, 1183 (1998).
20. R. V. Cadman et al., Phys. Rev. Lett. **86**, 967 (2001).
21. B. v. Przewoski et al., Phys. Rev. C **74**, 064003 (2006).
22. R. Bieber et al., Phys. Rev. Lett. **84**, 606 (2000).
23. J. Kuroś-Żołnierczuk et al., Phys. Rev. C**66**, 024003 (2002); Phys. Rev. C**66**, 024004 (2002).
24. W Pairsuwan et al., Phys. Rev. C **52**, 2552 (1995).
25. K. Hatanaka et al., Phys. Rev. C **66**, 044002 (2002).
26. Y. Maeda et al., Phys. Rev. C **76**, 014004 (2007).
27. H. Witała et al., Phys. Rev. C **71**, 054001 (2005).
28. H. Witała et al., in preparation.
29. H. Witała et al., Phys. Lett. **B 634**, 374 (2006).
30. R. Skibiński et al., Eur. Phys. J. A**30**, 369 (2006).
31. J. Golak et al., Phys. Rep. **415**, 89 (2005).
32. R. Skibiński, Ph.D. Thesis, Jagiellonian University, Kraków, 2002 (www.if.uj.edu.pl/ZFJ/prj.old-010501/fb/thesis2rs.html).
33. W. Tornow et al., Phys. Lett. **B 257**, 273 (1991).
34. D. I. Sober et al., Phys. Rev. C**28**, 2234 (1983).
35. N. M. O'Fallon, L. Koster Jr., J. Smith, Phys. Rev. C**5**, 1926 (1972).
36. M. A. Pickar et al., Phys. Rev. C**35**, 37 (1987).
37. T. Yagita et al., Mod. Phys. Lett. A**18**, 322 (2003).
38. E. Epelbaum, Prog. Part. Nucl. Phys. **57**, 654 (2006).